Defense Technical Information Center
Compilation Part Notice

ADP012167

TITLE: Nano-Structured Amporphous Carbon Films Synthesised Using DECR Plasma

DISTRIBUTION: Approved for public release, distribution unlimited

This paper is part of the following report:

TITLE: Materials Research Society Symposium Proceedings. Volume 675. Nanotubes, Fullerenes, Nanostructured and Disordered Carbon. Symposium Held April 17-20, 2001, San Francisco, California, U.S.A.

To order the complete compilation report, use: ADA401251

The component part is provided here to allow users access to individually authored sections of proceedings, annals, symposia, etc. However, the component should be considered within the context of the overall compilation report and not as a stand-alone technical report.

The following component part numbers comprise the compilation report:
ADP012133 thru ADP012173

NANO-STRUCTURED AMORPHOUS CARBON FILMS SYNTHESISED USING DECR PLASMA

André Golanski[1], Dieter Grambole [3], Jean Hommet [2], Folker Herrmann [3], Philippe Kern [1], Liam McDonnell [4], Fabrice Piazza [1] and Jean-Paul Stoquert [1]

[1] Centre National de la Recherche Scientifique (CNRS), Laboratoire PHASE,
B.P.20, F-67037 Strasbourg, France.
[2] Centre National de la Recherche Scientifique (CNRS), Laboratoire IPCMS
B.P. 20, F-67037 Strasbourg, France
[3] Forschungszentrum Rossendorf e.V., Institut für Ionenstrahlphysik und
Materialforschung
Postfach 51 01 19, 01314 Dresden, Germany
[4] Centre for Surface and Interface Analysis, Dept. of Applied Physics and Instrumentation,
Cork Institute of Technology
Rossa Av., Cork, Ireland

ABSTRACT

A Distributed Electron Cyclotron Resonance plasma reactor powered by a microwave generator operating at 2.45 GHz was used to deposit ta-C:H (Diamond-Like Carbon, DLC) thin films at RT. A graphite sputtering target immersed in an argon plasma was used as carbon source. The Ar plasma density was about 5×10^{10} cm^{-3}. Single crystal <100> Si substrates were RF biased to a negative voltage of -80 V. Atomic force microscopy (AFM), X-ray photoelectron spectroscopy (XPS), nuclear reaction analysis (NRA) using the resonance at 6.385 MeV of the reaction: $^{15}N + {}^{1}H \rightarrow {}^{12}C + {}^{4}He + \gamma$, elastic recoil detection analysis (ERDA) and Rutherford backscattering (RBS) were used to investigate the early phase of the growth. The morphology of the films grown at low pressure (0.3 mTorr) is shown to be dominated by stress-mediated nucleation leading to formation of basket-like clusters of circular hillocks 20 nm high surrounded by a planar, mostly sp^2 bonded film ~8 nm thick. With increasing plasma pressure the spatial frequency of the hillocks becomes random and the growth is dominated by the Stranski-Krastanov mode. The XPS data taken at decreasing emergence angles show that the structure of the hillocks is dominated by sp^3 bonded carbon. The XPS argon signal disappears at 10° emergence angle indicating that integration of argon occurs mainly within the sp^2 bonded regions. The NRA and ERDA analysis show that the amount of integrated hydrogen decreases with increasing substrate current density. RBS data indicate that increasing bias enhances argon integration.

INTRODUCTION

In the plasma deposition process where a negatively biased substrate is immersed in a carbon-rich plasma, the nucleation and growth are controlled by the flux and energy of the incoming species (charged and neutral). The results of the competition between integration of the incoming species and sputtering erosion depends on the precursor gas, ion energy and dose rate. Addition of argon to a carbon rich precursor such as acetylene is known to reduce the growth rate but momentum transfer being a forward-peaking process, argon bombardment may lead to a densification of the film and stress generation. Stress may in turn lead to transformation of sp^2 sites to sp^3 sites. Despite considerable experimental study over the last decade [1-6 and ref. therein] the effects of energy deposition on the morphology and physical properties of the DLC films are incompletely understood. The goal of the present work is to shed some more light on the impact of the energy deposition processes on the microstructure of the DLC thin films. The assumption here is that the binary collision theory may provide

some guidance as it enables assessment of the average energy density E_d deposited in binary collision cascades. Most of the experiments were performed using a constant substrate bias of -80 V corresponding to a maximum E_d value of ~14 eV/atom. The preliminary results reported below highlight the impact of the dose-rate effects on the materials structure.

EXPERIMENTAL DETAILS

Diamond-like amorphous carbon (DLC) thin films were deposited on single crystal <100> Si substrates using a plasma source operating in a Distributed Electron Cyclotron Resonance (DECR) configuration. The microwave power operating at a frequency of 2.45 GHz was applied to several antennae located in the vicinity of the cylindrical reactor walls that are equipped with magnetic racetracks designed to provide an appropriate confinement of fast electrons. At sufficiently low pressure (10^{-4} mTorr) the plasma diffuses under the influence of the density gradients and a uniformly distributed, cold, high density (~5×10^{10}/cm^3) diffusion plasma is obtained across the reactor volume. The plasma chamber was equipped with a water cooled graphite sputtering target located in the top part of the reactor and biased by a pulsed DC power supply producing negative voltage of tuneable amplitude. The graphite target and substrate to be coated were located at the opposite extremities of the reactor facing each other and immersed in the argon plasma. The substrate holder was water-cooled enabling the deposition temperature to be kept below 70°C for deposition time of a few minutes. The substrate bias of - 80 V was kept constant using a RF power supply operating at 13.5 MHz. The DLC films were analysed by atomic force microscopy (AFM), X-ray photoelectron spectroscopy (XPS), nuclear reaction analysis (NRA) using the resonance at 6.385 MeV of the reaction: $^{15}N + ^{1}H \rightarrow ^{12}C + ^{4}He + \gamma$ rays, elastic recoil detection analysis (ERDA) and Rutherford backscattering (RBS). The XPS analysis was performed using AlK$_\alpha$ (1486.6eV) X-ray radiation from a VG Microtech XR2E2 dual anode (aluminium/magnesium) X-ray source that was operated at 300 W power. XPS analysis was carried out using a VG Microtech VG100AX electron energy analyser. Angle resolved XPS spectra were obtained by rotating the sample holder with respect to the X-ray source and the input lens of the VG100AX analyser. Spectra were obtained for angles of emergence of photoelectrons from the surface of 90°, 70°, 50°, 30° and 10°. Data was acquired using VG Microtech VGX800 software and quantified using VG Microtech Presents software. XPS survey spectra were acquired using pass energy of 100 eV while high resolution spectra were acquired using a pass energy of 20 eV. No charge compensation has been used during acquisition.

RESULTS AND DISCUSSION

TABLE I and FIG.1 summarise the results of SRIM-2000 simulations performed for 80 eV Ar$^+$ ions in carbon, assuming the displacement energy for carbon atom to be of 15 eV. The average energy density E_d was estimated assuming a cylindrical geometry for an individual collision cascade. The radius of the cylinder was assumed to be of (R+σ_R) where R and σ_R are radial projected range and straggling, respectively. The length of the cylinder was assumed to be of 2.5 σ_L where σ_L is the longitudinal straggling of the Ar distribution. For the sake of simplicity the total ion energy was taken into account in the assessment of E_d. Yet, the maximum calculated E_d values are lower than the displacement threshold. The maximum E_d values are seen to correspond to the Ar$^+$ ion energy of 80 eV. We note that for the 80 eV C$^+$ ion the E_d value is almost an order of magnitude lower than for Ar$^+$ ion of the same energy. Most of the experiments reported in this work were performed using the substrate bias of U_S= −80V. The corresponding sputtering yield values shown in TABLE I indicate that
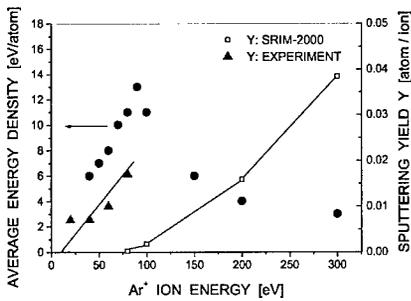
FIG.1: Deposited energy density and sputtering rate for Ar$^+$ ions measured experimentally and calculated using SRIM-2000
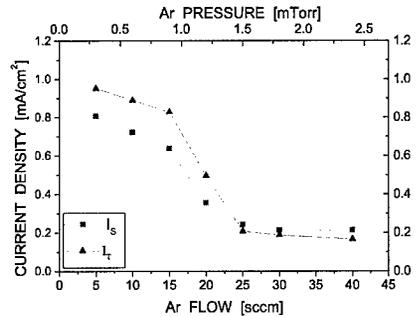
FIG.2: Substrate current density (I_S) and graphite target current density (I_T) plotted as a function of the argon pressure

TABLE I

	H$^+$	C$^+$	O$^+$	Ar$^+$	Experiment
Y [atoms C / ion]	0.010	0.044	0.014	<0.001	0.02
R$_p$ [Å]	19	7	6	7	

the combined sputtering effects due to the various ion species present in the plasma are expected to alter the morphology of the films [7]. Although no detailed diagnosis of the plasma has been performed at this stage the presence of hydrogen has been observed and is attributed to the desorption occurring at the reactor walls. The results of NRA and ERDA analysis (not shown) consistently indicate that while about 30 at.% hydrogen is observed in the film deposited using floating potential, the content is reduced by ion bombardment to 3-4 at.% in the films deposited using the substrate bias of -80 V. Given the significant deposition time (~30 min) the thermally activated, hydrogen ion induced surface erosion known to occur at process temperatures of T$\geq$400K may contribute to the total sputtering yield of Y=0.02 determined experimentally. The sputtering effects due to C$^+$ and Ar$^+$ ions are expected to be of a similar order of magnitude because the population of carbon ions within the plasma is estimated to be about 1% of the Ar$^+$ ion population.

FIG.2 shows the substrate and graphite target current densities (I_S and I_T, respectively) plotted as a function of the argon plasma pressure. Secondary electron emission is not taken into account in the assessment of the current density. It is assumed to be negligible for the ion energies used [8]. The current density values I_S and I_T are close to one another and decrease with increasing argon pressure, reflecting the relative density of the charged and neutral species within the plasma. Consequently the substrate current density may be varied by changing the plasma pressure. In the experiments reported in this work the DLC films were grown during 30 min using variable current density I_S. The deposition parameters are shown in Table II. We note that the results of RBS analysis (spectra not shown) indicate that when

TABLE II

	Pressure [mTorr]	Dose rate [10^{15} ions/cm^{2}s]	Total dose [10^{19} ions/cm^2]
FIG. 3 a	0.1	13	2.3
FIG. 3 b	0.2	9.4	1.5
FIG. 3 c	0.9	6.2	1.1
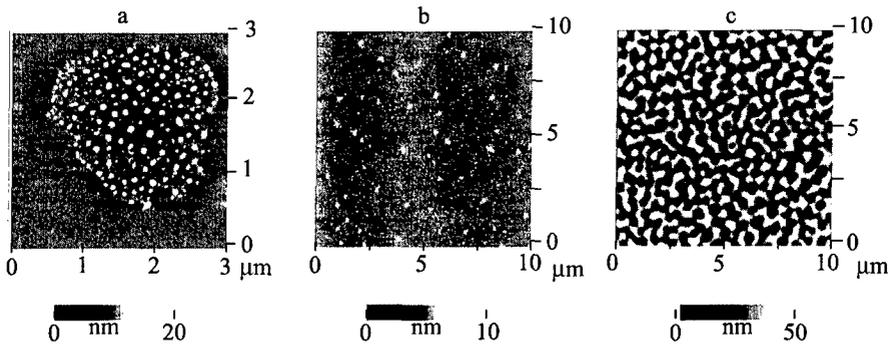
FIG.3 : AFM images of the films deposited using constant energy of 80 eV and variable dose-rate of 1.3×10^{16} (a), 9.4×10^{15} (b) and 6.2×10^{15} (c) [Ar^+ ions/cm^{2}s]

the substrate bias is increased from 0 V to -80 V, the residual argon content increases from zero to about 6 at.%. More than 99% of the argon atoms reaching the growing film is re-sputtered and/or disrobed during the growth.

The relationship between the dose, dose rate and the surface topography and microstructure of the film was investigated using AFM and XPS techniques. The AFM images corresponding to three different I_S values are shown in FIG.3.

The AFM image corresponding to the highest dose rate (FIG.3a) reveals that most of the DLC surface is flat. It also reveals the presence of a variety of self-organised, basket-like clusters of densely packed circular hillocks. The clusters are distributed randomly and separated from one another by a distance of several tenths of microns. The hillocks within the cluster are of various sizes reaching 20 nm in height. The auto-correlated, basket-like networking is believed to result from a strain-mediated nucleation and growth processes. Khachaturyan [9] discussed the corresponding mechanism. Unlike the conventional thermodynamic theory of phase transformations, Khachaturyan's approach includes stress energy contributions to the free energy of the system. The growing nucleus is seen as generating a stress field where the surface energy and the nucleation probability are enhanced. The latter effect leads to a directional ordering and mutual arrangement of the nuclei and eventually results in the formation of a partially ordered, "basket-like" pattern of hillocks where the stress energy of the whole structure is reduced.

The initial stress field required for the stress mediated nucleation to occur is tentatively attributed to high dose-rate effects enabling neighbouring binary collision cascades to overlap, creating high deposited energy density (~30 eV/atom) regions and leading to a significant redistribution of atomic bonds. The effects of cascade overlap have been investigated in the keV energy range and shown to lead to a non-linear enhancement in both damage creation and sputtering [9]. Taking into account the average space frequency of the basket-like patterns of ~1×10^{-4} /μm^2 observed for the dose rate of 1.3×10^{16} ions/cm^{2}s, an ion flux of 10^{16} ions/cm^{2}s represents a threshold value beyond which the 80 eV Ar ions cascade overlap effects become observable. At lower dose rates the effects are expected to vanish.

When the dose rate is reduced to 9.4×10^{15} [ions/cm^{2}s] the AFM image becomes dominated by a random network of individual hillocks (FIG.3b). The film appears to grows in the Stranski-Krastanow mode. Although the basket-like clusters are still observed, their spatial frequency

is significantly lower. The average density of hillocks in FIG. 3b is an order of magnitude lower than within a cluster (FIG.3a).

When the ion dose rate is further reduced to 6×10^{15} [ions/cm^{2}s] the surface erosion is also significantly reduced and the topography of the surface changes significantly (FIG.3c). The hillocks are now present all over the surface. They reach 50 nm in height and a significant degree of overlap is observed (FIG.3c). The average density of hillocks in FIG. 3b and 3c is similar, but they are different in size. Figures 3b and 3c are interpreted as corresponding to a similar nucleation dynamics and different stages of growth. Although the integrated ion dose is smaller for FIG. 3c, the corresponding average layer thickness is higher.

The samples shown in FIG. 3b and 3c were analysed using the XPS technique. The Ar/C signal ratio has been investigated as a function of the emergence angle. The results are summarised in FIG.4. The straight lines have been added to underline the trends. With decreasing angle of emergence the argon peak falls off faster than the overall carbon peak. Argon is not seen at the glancing angle indicating that the argon rich layer is buried underneath the surface. The difference in glancing angle at which the Ar signal disappears is attributed to the difference in depth Δx at which the argon reach layer is buried. Since a constant energy of 80 eV is used in this experiment, the values of Δx are believed to depend on the film density. A simple calculation shows that Δx(FIG.3c)/Δx(FIG.3b)$\approx$0.5. The relationship between the projected range for 80 eV Ar$^+$ and DLC density extracted from SRIM (FIG.5) indicates that the corresponding change in density is of about 1.2 g/cm^3. According to [5,6] an increase in density of 0.5 g/cm^3 corresponds to an increase in the sp^3-hybridised fraction of 25%. Consequently the sample shown in FIG.3c is expected to contain a significantly higher sp^3 fraction than the sample shown in FIG. 3b. The XPS analysis confirms the expectations. Implanted or subimplanted argon atoms have been shown to probe the residual stress in ultrathin films since intrinsic stress induces a change in the binding energy of Ar2p electrons. The change, measurable by the XPS technique, is linearly proportional to the stress [11]. XPS analysis shows a 0.3 eV difference in the binding energy of Ar2p electrons between the two samples shown in FIG. 3b and 3c with the latter showing the higher stress. The carbon hybridisation ratio corresponding to the film shown in FIG.3c has been analysed by peak fitting of the C1s feature in the XPS spectra (not shown). Following a detailed consideration of the prior work the C1s feature was fitted using four components that include sp^2 and sp^3 hybridisation and two chemical states associated with oxygen.
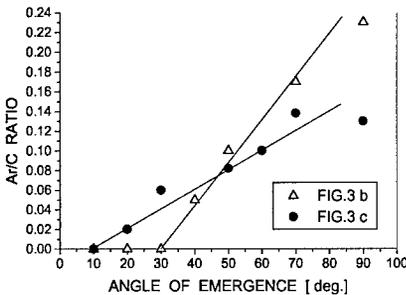
FIG.4: XPS Ar/C signal ratio for the samples shown in FIG. 3b and 3c.
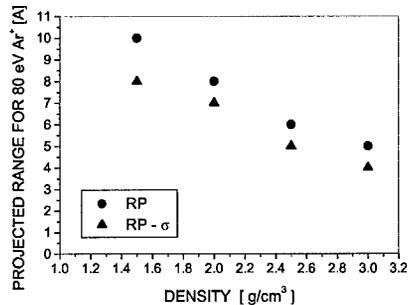
FIG.5: 80 eV Ar$^+$ ion range plotted as a function of carbon density [SRIM 2000]

The hybridisation analysis shows that the sp^3 ratio increases as the angle of emergence decreases thereby indicating that sp^3 carbon is outermost within the film structure. This result strongly suggests that sp^3 rich hillocks reside in a sp^2 rich "ocean". The fact that the XPS argon signal disappears at 10° emergence angle may also indicate that integration of argon occurs mainly within the sp^2 bonded regions. Assuming that the hillocks seen in FIG.3a are also sp^3 rich we tentatively conclude that the resistance to the surface etching by ion bombardment depends on hybridisation. Further study is required to confirm these preliminary conclusions.

CONCLUSIONS

We have provided experimental evidence that the surface topography and microstructure of the plasma deposited ta-C:H thins films strongly depend on the substrate current density. We have demonstrated that for ta-C:H films grown on a single crystal Si substrate the high dose rate effects may lead to a stress-mediated nucleation. Finally, we have shown that integration of argon within ta-C:H is enhanced by Ar^+ ion energy and occurs mainly within the sp^2 hybridised carbon fraction.

ACNOWLEDGMENTS

REFERENCES
1. W.Lu, K.Komvopoulos and S.W.Yeh, J.Appl.Phys. 89, 4 (2001)
2. L.Valentini, J.M.Kenny, G.Carlotti, G.Socino, L.Lozzi and S.Santucci, J.Appl.Phys. 89, 2 (2001)
3. A.Ilie, A.Hart, A.J.Flewitt, J.Robertson and W.I.Milne, J.Appl.Phys. 88, 10, 6002 (2000)
4. R.G.Lacerdaz, P.Hammer, F.L.FreireJr, F.Alvarez and F.C. Marques, Diamond and Related Materials 9, 796 (2000)
5. D.H.Lee, X.M.He, K.C.Walter, M.Nastasi, J.R.Tesmer and M.Tuszewski, Appl.Phys.Letters 73, 17, 2423 (1998)
6. J.Schwan, S.Ulrich, H.Roth, H.Ehrhardt, S.R.P.Silva, J.Robertson, R.Samlenski and R.Brenn, J.Appl.Phys. 79, 3, 1416 (1996)
7. W.Jacob, Thin Solid Films 326, 1 (1998)
8. E.S.Parilis et al., Atomic Collisions on Solid Surfaces, North-Holland, Amsterdam (1993)
9. A.G.Khachaturian, Theory of Structural Transformations in Solids, John Willey&Sons 1983 (ISBN 0-471-07873-5)
10. D.A.Thompson, Radiation Effects 56, 105-150 (1981)
11. A.LiBiassi, A.C.Ferrari, V.Stoloian, B.K.Tanner, J.Robertson and L.M.Brown, Diamond and Related Materials 9, 771 (2000)
12. W.Lu and K.Komvopulos, Appl.Phys.Letters 76, 22, 3206 (2000)